Application of the Time-Varying Koopman Operator for Bifurcation Analysis in Hypersonic Aerothermoelasticity

Damien Guého*, Daning Huang†, Puneet Singla‡
Department of Aerospace Engineering, Pennsylvania State University, Univeristy Park, PA-16802

A time-varying Koopman operator (TVKO) is presented to study the nonlinear coupled dynamics between structural dynamics, heat transfer, and hypersonic aerothermodynamics, viz. AeroThermoElasticity (ATE). TVKO can be considered as an extension of the classical time-invariant Koopman operator (TIKO). It utilizes a subspace realization method known as the time-varying Eigensystem Realization Algorithm (TVERA) to approximate the underlying nonlinear model as a time varying linear model in a lifting space from time histories of input-output data. A benchmark model depicting the complex ATE dynamics for the flutter of a heated panel is considered to show the efficacy of the presented approach. The numerical experiments performed demonstrate the accuracy of the presented approach in capturing the bifurcation behavior in limit cycle oscillations due to variations in dynamic pressure.

I. Introduction

Air-breathing hypersonic vehicles are under increasingly active development in the recent years [1, 2]. This class of vehicles are expected to operate at high Mach number in the atmosphere for the entire mission profile that can last for 30 minutes or longer. Due to the high speeds and the resulting extreme aerothermodynamic environment, it is well-known to the community that the coupling between the structural dynamics, heat transfer, and hypersonic aerothermodynamics, viz. aerothermoelasticity (ATE), constitutes the core subsystem governing the operation of a hypersonic vehicle. However, due to the current limited capability of ground tests and the lack of available flight test data, there is a significant degree of uncertainty associated with the ATE modeling of hypersonic vehicles and limited ability to alleviate this uncertainty through experimental testing [3–5]. Significant algorithmic development is required to identify, quantify, and propagate these stochastic effects and model errors through a time-dependent, high-dimensional state space, as is the case for hypersonic ATE analysis. The predictive aerothermoelastic capability *with uncertainty* over extended flight time is a key ingredient for analyzing performance, stability, and reliability of hypersonic vehicles.

Currently, the aerothermoelastic analysis is typically performed using an aerothermal surrogate coupled to nonlinear finite element (FE) models for structural dynamics and heat transfer, i.e. the thermoelastic solver [6–8]. The nonlinearity in the FE models is critical for capturing the bifurcation-induced instabilities in ATE responses, such as buckling and panel flutter. The uncertainty quantification and propagation in a nonlinear thermoelastic model is challenging in general, especially in the presence of bifurcations. As a step towards efficient uncertainty quantification in ATE analysis, we propose to derive a *linear* reduced-order model (ROM) using a recently-developed system identification formalism. These ROMs act as high-dimensional nonlinear thermoelastic solvers in conventional ATE analysis, while *retaining* the bifurcation characteristics of the original system. Once such a linear ROM becomes available, the UQ of ATE analysis over extended time will become tractable.

Recent advances in nonlinear system identification have used the Koopman operator theoretic approach to obtain precise predictions of a nonlinear dynamical system as the output of a truncated linear dynamical system. The main idea behind Koopman operator theory [9, 10] is to lift the nonlinear dynamics into a higher dimensional space where the evolution of the system is linear. The resulting operator, called the Koopman operator, is a infinite-dimensional linear operator that governs the evolution of scalar functions, i.e. the measurements of the nonlinear system. Even though the core challenge of the Koopman operator theoretic approach is to specify (directly or indirectly through decompositions) the Hilbert space of measurement functions of the state of the system, the theory has been applied for uncontrolled [11, 12] and controlled systems [13, 14] with promising results using popular subspace realization methods such as dynamic mode decomposition (DMD) and its extensions [15]. Since then, DMD has had countless other variants with some of the most popular being Regular-DMD [16], Exact-DMD [17], and Extended-DMD (eDMD) [18].

*PhD Candidate, Student Member AIAA, Email: djg76@psu.edu.
†Assistant Professor, AIAA Member, Email: daning@psu.edu.
‡Professor, AIAA Associate Fellow, AAS Fellow, Email: psingla@psu.edu.

Non-eDMD methods attempt to find the best-fit linear model which advances measurements forward one time step. Constructing the Koopman operator from these linear measurements, however, is often not "rich" enough for some nonlinear systems. Unlike non-eDMD methods, eDMD instead uses nonlinear measurements of the state based on a predetermined dictionary. However, eDMD truly only approximates the Koopman operator projected onto the chosen dictionary of functions [13]. In fact, if the chosen lifted space is not a Koopman-invariant subspace, eDMD may produce some illegitimate spectral elements. It has been shown for systems with multiple fixed points that directly includes the raw state measurement in the DMD model will effectively nullify the possibility of finding a finite-dimensional Koopman subspace [14]. More importantly, the resulting linear operator is a local approximator of the nonlinear dynamical system valid in the neighborhood of a nominal point and the domain of validity of this local linear approximation improves as the dimension of the lifting space is increased. However, one may need a very large dimensional lifting space to accurately capture the flow of the underlying nonlinear system.

An alternative to improve the validity region of the Koopman operator and curtail the dimension of the lifting space is to consider the linearization of the nonlinear flow about a nominal trajectory of the nonlinear system rather than a nominal point. The linearization about a nominal trajectory leads to a linear time-varying (LTV) system as opposed to a linear time-invariant (LTI) system for the conventional Koopman operator. However, LTV systems exhibit distinct properties, as compared to the shift invariance exhibited by LTI systems. All the subspace methods for LTI system identification exploit the fact that an infinity of system realizations exist and actually share the same Markov parameters (also known as system impulse response functions) and the eigenvalues of the state transition matrix. However, no such property exists for the LTV system. The lack of similarity transformations handicap the application of conventional subspace methods such as DMD to identify LTV systems. The literature in linear time varying system identification [19–26] is limited as compared to LTI system identification by the fact that there are no approaches to find similarity transformations between the model sequences. In our earlier work [24, 25], it is shown that there exist special reference frames, in which the identified models are similar to the true model, i.e., state transition matrices share the same eigenvalues. Using this key result the realizations can be compared across different data sets. This forms the basis for spectral characterization of the time varying systems and the resulting algorithm is known as the time-varying eigensystem realization algorithm (TVERA). By exploiting the TVERA formulation in conjunction with the idea of a lifted measurement space, this manuscript describes the procedure to derive a time-varying Koopman operator (TVKO) [27].

This paper aims to demonstrate the capabilities of the TVKO approach to provide a LTV model to reproduce the aerothermoelastic response of a hypersonic vehicle. This eventually will enable accurate hypersonic aerothermoelastic analysis and control with tractable computational cost. Specifically, the objectives are,

1) Present the TVERA algorithm for obtaining linear ROMs from measurements of nonlinear systems,
2) Benchmark the capabilities and performance of the TVKO and TIKO (time-invariant Koopman operator) models using an academic problem such as the analytical heated panel flutter model.
3) Apply the reduced-order modeling algorithms to perform bifurcation analysis of the flutter problem.

The paper's organization is as follows: Section II introduces the Koopman operator theory for autonomous systems in a time-varying setting. Section III provides a detailed description of the implementation procedure to obtain an approximation of this time-varying operator. To validate the developed approach, Section IV considers a numerical simulation involving the nonlinear dynamics of a simple heated panel model.

II. Problem Statement

Let's consider a parametric initial value problem in a state space form

$$\dot{\boldsymbol{x}} = \boldsymbol{f}(t, \boldsymbol{x}; \boldsymbol{u}), \quad \boldsymbol{x}(0) = \boldsymbol{x}_0, \tag{1}$$

where $\boldsymbol{x} \in \mathbb{R}^n$ is the state of the system (also usually the *unknown* minimal set of variables needed to describe the evolution of the system) and $\boldsymbol{f}$ is a function of a vector field that describes how the system changes at a given state in time, and $\boldsymbol{u} \in \mathbb{R}^m$ is the bifurcation parameter. The basic idea of TVERA is to generate time-varying linear models for the nonlinear system for each set of fixed parameters; for new parameters, an interpolation is required to generate the corresponding new linear models. In this section, the general Koopman operator theory for an autonomous system is first described; subsequently, the general theory is presented in a form amenable for TVERA development.

A. Koopman Operator for Autonomous Systems

First, the basic properties of the continuous-time Koopman operator are discussed. Consider an autonomous nonlinear dynamical system,

$$\dot{\boldsymbol{x}} = \boldsymbol{f}(\boldsymbol{x}(t)), \quad \boldsymbol{x}(0) = \boldsymbol{x}_0 \tag{2}$$

where $t \in \mathbb{R}$, $\boldsymbol{x} \in \mathbb{X} \subseteq \mathbb{R}^n$, $\boldsymbol{f} : \mathbb{X} \to \mathbb{R}^n$. Assuming the system has a unique solution, and consequently its inverse, existing over any time interval, Eq. (2) has an associated continuous-time flow map $\mathbf{F}_c$ defined in Eq. (3a) and satisfies group properties defined in Eq. (3b), where $\mathbf{F}_c^t : \mathbb{X} \to \mathbb{X}$.

$$\boldsymbol{x}(t) = \mathbf{F}_c^t(\boldsymbol{x}_0) = \boldsymbol{x}_0 + \int_0^t \boldsymbol{f}(\boldsymbol{x}(t))dt \tag{3a}$$

$$\forall t, s \in \mathbb{R}, \quad \mathbf{F}_c^t \circ \mathbf{F}_c^s(\,\cdot\,) = \mathbf{F}_c^{t+s}(\,\cdot\,), \quad \mathbf{F}_c^0(\,\cdot\,) = \mathcal{I}, \tag{3b}$$

The continuous-time Koopman operator $\mathcal{K}_c$ is defined generally as an infinite-dimensional linear operator that advances some complex-valued measurement function $\chi : \mathbb{X} \to \mathbb{C}$ through,

$$\chi(\boldsymbol{x}_t) = \mathcal{K}_c^t \chi(\boldsymbol{x}_0) = \chi \circ \mathbf{F}_c^t(\boldsymbol{x}_0) \tag{4}$$

where $\mathcal{K}_c^t : \mathcal{F} \to \mathcal{F}$, and $\chi(\mathbf{x})$ is a measurement function in the Hilbert space $\mathcal{F}$. Eq. (4) defines the Koopman operator as a unitary infinite-dimensional linear operator acting on the measurement functions. It is also important to note that the Koopman operator is a member of the continuous one-parameter unitary group of operators $\{\mathcal{K}_c^t\}_{t\in\mathbb{R}}$ generated by the *Koopman generator U* defined by Eq. (5a), provided the limit exists [28]. The Koopman operator in this setting is also said to satisfy the group properties defined in Eq. (5b),

$$U\chi = \lim_{\Delta t \to 0} \frac{\mathcal{K}_c^{\Delta t}\chi - \chi}{\Delta t} = \lim_{\Delta t \to 0} \frac{\chi \circ \mathbf{F}_c^{\Delta t} - \chi}{\Delta t}, \tag{5a}$$

$$\forall t, s \in \mathbb{R}, \quad U^t \circ U^s(\,\cdot\,) = U^{t+s}(\,\cdot\,), \quad U^0(\,\cdot\,) = \mathcal{I} \tag{5b}$$

If the measurement functions are differentiable, Eq. (5a) indicates that the Koopman generator applied to a measurement function χ is the time derivative of the measurement, $\dot{\chi}$, and

$$U\chi = \frac{d}{dt}\chi(\boldsymbol{x}(t)) = \frac{d\chi}{d\boldsymbol{x}}\frac{d\boldsymbol{x}}{dt} = \boldsymbol{f}(\boldsymbol{x}) \cdot \nabla_{\boldsymbol{x}}\chi. \tag{6}$$

Note that in general, the Koopman generator may have a continuous spectrum, which effectively makes the system dynamic chaotic and challenging for ML-based approximations. In this study, it is assumed that the Koopman generator has a spectrum dominated by discrete eigenvalues, which is practical for many engineering applications [29–32]. The assumption indicates that the Koopman generator can be decomposed spectrally into a *fixed set* of eigenvalue-eigenfunction pairs (λ_i, ψ_i),

$$U\psi_i = \lambda_i \psi_i. \tag{7}$$

where $\lambda_i \in \mathbb{C}$, $\psi : \mathbb{X} \to \mathbb{C}$, $\psi \in \mathcal{F}$, and $i = 1, 2, ..., \kappa$ or ∞. If the eigenfunctions of the Koopman generator are used as the measurement functions, then the dynamics of the linear system Eq. (4), i.e. the Koopman operator, is solely determined by the eigenvalues.

With the discussion of the continuous-time Koopman operator, it is natural to introduce its discrete-time counterpart. First, let $\boldsymbol{F}$ be the discrete-time flow of the dynamical system that maps the state from one time to the other, with a time step size Δt

$$\boldsymbol{x}_{k+1} = \boldsymbol{F}(\boldsymbol{x}_k) \tag{8}$$

with $\boldsymbol{x}_k = \boldsymbol{x}(k\Delta t)$. Let $\boldsymbol{\chi}(\boldsymbol{x})$ be a set of measurements in the Hilbert space $\mathcal{F}$, the infinite-dimensional Koopman operator $\mathcal{K}$ provides a linear operator for the transition of these measurements forward in time, i.e.,

$$\boldsymbol{\chi}_{k+1} = \mathcal{K}\boldsymbol{\chi}_k, \tag{9}$$

where

$$\boldsymbol{\chi}_k = \begin{bmatrix} \chi_k^1 \\ \chi_k^2 \\ \vdots \end{bmatrix} = \boldsymbol{\chi}(\boldsymbol{x}_k) \tag{10}$$

Each $\chi_k^i = \chi^i(\boldsymbol{x}_k)$, $i = 1, 2, \ldots$, is assumed to be observable in $\mathcal{F}$. Note that Eq. (9) provides an infinite dimensional LTI system version of the nonlinear flow of Eq. (8) in the measurement space $\mathcal{F}$. Since $\boldsymbol{\chi}_{k+1} = \boldsymbol{\chi}(\boldsymbol{x}_{k+1}) = \boldsymbol{\chi}(\boldsymbol{F}(\boldsymbol{x}_k))$, one can write

$$\mathcal{K}\boldsymbol{\chi}_k = \boldsymbol{\chi}_k \circ \boldsymbol{F}. \tag{11}$$

The continuous-time and discrete-time Koopman operators are connected by

$$\mathcal{K} = \mathcal{K}_c^{\Delta t} \tag{12}$$

and by Koopman-Kolmogorov theorem [33] the eigenvalue-eigenfunction pairs of the discrete-time Koopman operator are $(e^{\lambda_i \Delta t}, \psi_i)$.

$$\mathcal{K}\psi_i = \mathcal{K}_c^{\Delta t}\psi_i = e^{\lambda_i \Delta t}\psi_i \tag{13}$$

The Koopman operator is shown to fully capture all properties of the underlying nonlinear dynamical system, provided that the state vector $\boldsymbol{x}_k$ is observable from the lifted space measurements generated by $\boldsymbol{\chi}_k$ [11, 12], with a trading between nonlinear dynamics in a finite-dimensional space and linear dynamics in a potentially infinite-dimensional lifted space. Figure 1 offers a general view of the Koopman operator theoretic framework.

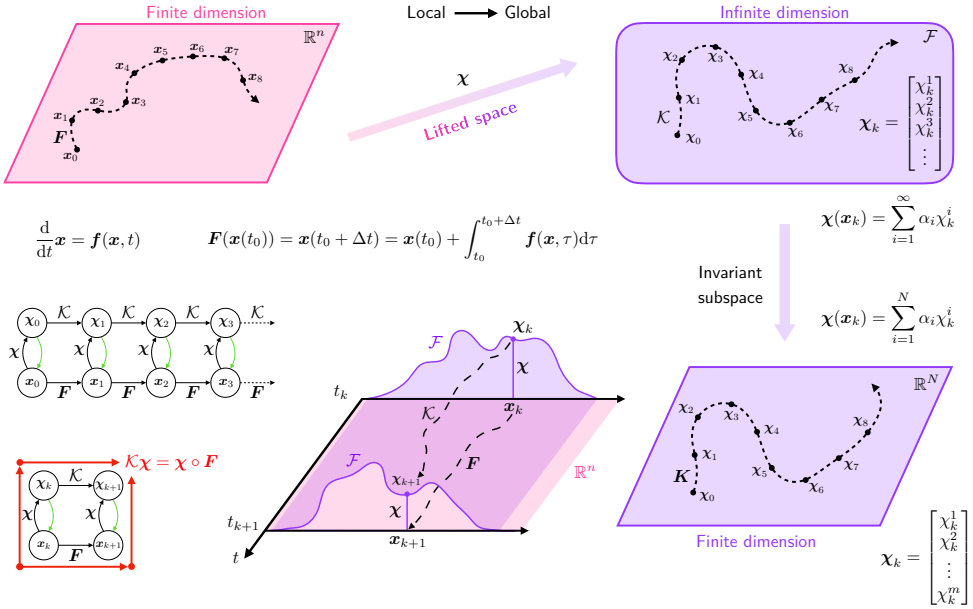

Fig. 1 Global representation of the Koopman operator theoretic framework

B. Time-varying Koopman Operator

Though the Koopman operator is usually infinite dimensional, the measurement vector $\boldsymbol{\chi}_k$ is truncated to finite dimension $N >> n$ for numerical simulation purposes. In order to obtain a linear prediction model, the following structure for $\boldsymbol{\chi}_k$ is assumed:

$$\boldsymbol{\chi}_k(\boldsymbol{x}_k) = \begin{bmatrix} \boldsymbol{x}_k \\ \boldsymbol{\Theta}(\boldsymbol{x}_k) \end{bmatrix}. \tag{14}$$

where $\boldsymbol{\Theta}(\boldsymbol{x}_k)$ represents the mapping of the dynamical system states in the lifted space. In TVERA, the states of the nonlinear system, $\boldsymbol{x}_k$, are included as the first n components of $\boldsymbol{\chi}_k$, leading the dynamical system of Eq. (9) to be fully observable at each time step. Now, the problem of finding the Koopman operator can be restated as the identification of the following LTI system given the time histories of $\boldsymbol{\chi}_k$:

$$z_{k+1} = Az_k \tag{15}$$

$$\hat{\boldsymbol{\chi}}_k = Cz_k \tag{16}$$

Generally, z_k is assumed to be a N-dimensional hidden state vector corresponding to the Koopman dynamics, however, one can also estimate the dimension of z_k as part of the identification process. $\hat{\chi}_k$ is the estimated measurement vector and the estimate for the state of the nonlinear system, denoted by $\hat{x}_k$, can be extracted from the first n components of $\hat{\chi}_k$. The observable pair of unknown system matrices (A, C) is found such that the norm of the measurement error $\|\chi_k - \hat{\chi}_k\|$ is minimized. Conventional subspace decomposition methods such as the Eigensystem Realization Algorithm (ERA) [17, 34, 35] or Dynamic Mode Decomposition (DMD) [16, 36, 37] are used to provide an *observable* realizations for the system matrices (A, C), hence performing a linearization about a single point of the dynamical system in the lifted space. In earlier work [11–15], it is shown that the state prediction error improves as the dimension of the lifted space, N is increased. Generally, N needs to be much larger than state dimension n for the Koopman operator to provide a good prediction of the system states.

In this work, a time-varying Koopman operator is developed as an alternate means to increase the prediction accuracy for a fixed dimension of the lifted space, i.e.,

$$\chi_{k+1} = \mathcal{K}_k \chi_k. \tag{17}$$

The identification of a time varying Koopman operator corresponds to finding a LTV system in the lifted space such that

$$z_{k+1} = A_k z_k \tag{18}$$

$$\hat{\chi}_k = C_k z_k. \tag{19}$$

Development of methods for time-varying systems have involved recursive and fast implementations of time invariant methods by exploring structural properties of the input–output realizations [38] or by generalizing several concepts in classical linear time invariant system theory consistently [19, 20]. More recent efforts [26] have concentrated on extending LTI subspace realizations methods by considering moving time windows and weighting factors on the data sequence or introducing explicit parameters to take into account the time-varying amplitude of the corresponding modes during the decomposition phase of the algorithm [39]. However, these efforts suffer from the lack of a method to find similarity transformations between the model sequences for LTV systems, as well as to relate the identified model to the true linear dynamics. If there were different coordinate systems defined by the Lyapunov transformation $w_k = T_k z_k$ whose state space realization is given by $w_{k+1} = F_k w_k$, along with $\hat{\chi}_k = H_k w_k$, then the realizations A_k, F_k are NOT similar. This is in sharp contrast to the LTI theory, where a variety of realizations (all infinity of them, that share the same Markov parameters) share the same spectrum. In Refs [24, 25], it is shown that there exists special reference frames in which the models are similar, i.e., $\tilde{A}_k, \tilde{F}_k$ share the same eigenvalues. This special reference frame can be determined from observability matrices corresponding to different realizations of the system matrices. The resulting algorithm is known as TVERA and the next section discusses its application to obtain the time-varying Koopman operator.

III. Identification of the time-varying Koopman operator from Data

This section details the TVERA algorithm to obtain a time-varying Koopman approximator for a nonlinear system response from the time history of measurements in the lifted-space obtained from repeated experiments. In this development, it is assumed these experiments are associated with the same fixed bifurcation parameter. The idea of repeated experiments has been introduced in [21, 40] and presented as practical methods to realize conceptual time-varying state space model identification strategies. From a perspective of generalizing the LTI subspace methods to the case of time-varying systems, a time-varying version of ERA has been developed in [24]. Additionally, it has been showed that the generalization thus made enables the identification of time-varying plant models that are in arbitrary coordinate systems at each time step and a time-varying transformation is derived to convert system states at different time into one common frame if necessary. This section summarizes the key ideas of the TVERA algorithm and one should refer to [24] for more details on TVERA.

To get insight into the TVERA process, let us consider the solution of the difference equation of Eq. (17)

$$\chi_k = C_k \Phi(k, 0) z_0 \tag{20}$$

where $\Phi(k, i+1)$ is the state-transition matrix defined as

$$\Phi(k, k_0) = \begin{cases} A_{k-1} A_{k-2} \dots A_{k_0} & \text{for } k > k_0, \\ I & \text{for } k = k_0, \\ \text{undefined} & \text{for } k < k_0. \end{cases} \tag{21}$$

The method for computing the system matrices using a set of experimental data $\{\boldsymbol{\chi}^{\#i}\}_{i=1..m}$ (free response experiments) involves the construction of the matrix $\tilde{\boldsymbol{H}}_k^{(p,m)}$,

$$\tilde{\boldsymbol{H}}_k^{(p,m)} = \begin{bmatrix} \boldsymbol{\chi}_k^{\#1} & \boldsymbol{\chi}_k^{\#2} & \cdots & \boldsymbol{\chi}_k^{\#m} \\ \boldsymbol{\chi}_{k+1}^{\#1} & \boldsymbol{\chi}_{k+1}^{\#2} & \cdots & \boldsymbol{\chi}_{k+1}^{\#m} \\ \vdots & \vdots & \ddots & \vdots \\ \boldsymbol{\chi}_{k+p-1}^{\#1} & \boldsymbol{\chi}_{k+p-1}^{\#2} & \cdots & \boldsymbol{\chi}_{k+p-1}^{\#m} \end{bmatrix} = \boldsymbol{O}_k^{(p)} \boldsymbol{Z}_k^{(m)}, \tag{22}$$

where $\boldsymbol{O}_k^{(p)}$ is the observability matrix at time k

$$\boldsymbol{O}_k^{(p)} = \begin{bmatrix} C_k \\ C_{k+1}A_k \\ C_{k+2}A_{k+1}A_k \\ \vdots \\ C_{k+p-1}A_{k+p-2}\ldots A_k \end{bmatrix}, \tag{23}$$

and $\boldsymbol{Z}_k^{(m)}$ is a state variable ensemble matrix at time k:

$$\boldsymbol{Z}_k^{(m)} = \begin{bmatrix} \Phi(k,0)z_0^{\#1} & \Phi(k,0)z_0^{\#2} & \cdots & \Phi(k,0)z_0^{\#m} \end{bmatrix} \in \mathbb{R}^{N\times m}. \tag{24}$$

The state variables $z_0^{\#1}, z_0^{\#2}, \ldots, z_0^{\#m}$ are simply the initial conditions from where the free response experiments are derived. The parameter p and the number of free response experiments m are chosen such that the matrix $\tilde{\boldsymbol{H}}_k^{(p,m)}$ retains the rank N, the dimension of the lifted space of measurements. Indeed, if $pN \geq N$ and $m \geq N$, matrices $\boldsymbol{O}_k^{(p)}$ and $\boldsymbol{Z}_k^{(m)}$ are of rank maximum N (equal to N for $\boldsymbol{Z}_k^{(m)}$). If the system is observable, the block matrix $\boldsymbol{O}_k^{(p)}$ is of rank exactly N and so is $\tilde{\boldsymbol{H}}_k^{(p,m)}$. Identifying the number of dominant singular values of the Hankel matrix will thus provide an indication about the unknown order of the reduced model to be identified. If the rank of the Hankel matrix is less than N, it will then be equal to the rank of the completely observable subspace. Differing ranks are possible for this generalized time-varying matrix $\tilde{\boldsymbol{H}}_k^{(p,m)}$ at every time step for the variable state dimension problem. In this work, it is assumed that the dimension of the lifted space does not change with the time index. However, this assumption can be relaxed without much difficulty.

As for the general procedure in ERA or TVERA, the singular value decomposition of $\tilde{\boldsymbol{H}}_k^{(p,m)}$ allows for the identification of the current observability and ensemble matrices,

$$\tilde{\boldsymbol{H}}_k^{(p,m)} = \boldsymbol{U}_k \boldsymbol{\Sigma}_k \boldsymbol{V}_k^{\intercal} = \begin{bmatrix} \boldsymbol{U}_k^{(N)} & \boldsymbol{U}_k^{(0)} \end{bmatrix} \begin{bmatrix} \boldsymbol{\Sigma}_k^{(N)} & \boldsymbol{0} \\ \boldsymbol{0} & \boldsymbol{\Sigma}_k^{(0)} \end{bmatrix} \begin{bmatrix} \boldsymbol{V}_k^{(N)\intercal} \\ \boldsymbol{V}_k^{(0)\intercal} \end{bmatrix} \tag{25a}$$

$$= \boldsymbol{U}_k^{(N)} \boldsymbol{\Sigma}_k^{(N)} \boldsymbol{V}_k^{(N)\intercal} + \underbrace{\boldsymbol{U}_k^{(0)} \boldsymbol{\Sigma}_k^{(0)} \boldsymbol{V}_k^{(0)\intercal}}_{\simeq \boldsymbol{0}} \tag{25b}$$

$$\simeq \boldsymbol{U}_k^{(N)} \boldsymbol{\Sigma}_k^{(N)} \boldsymbol{V}_k^{(N)\intercal} \tag{25c}$$

where the approximation at a given time step k is made possible by rejecting the small singular values. Indeed, some singular values of $\boldsymbol{\Sigma}_k$ may be relatively small and negligible, in the sense that they contain more noise information than system information. Hence, the approximation $\boldsymbol{U}_k^{(0)} \boldsymbol{\Sigma}_k^{(0)} \boldsymbol{V}^{(0)\intercal}{}_k \simeq \boldsymbol{0}$ (truncation of nonzero small singular values) is to account for noise in the data and for quantitatively partitioning the realized model into principal and perturbation (noise) portions so that the noise portion can be disregarded. In other words, the directions determined by these singular values have less significant degrees of observability relative to noise. The derived model of order N after deleting these singular values is then considered as the robustly observable part of the realized system. In terms of the corresponding observability and state variable ensemble matrices,

$$\tilde{\boldsymbol{H}}_k^{(p,m)} = \boldsymbol{U}_k^{(N)} \boldsymbol{\Sigma}_k^{(N)} \boldsymbol{V}_k^{(N)\intercal} = \boldsymbol{O}_k^{(p)} \boldsymbol{Z}_k^{(m)} \Rightarrow \begin{cases} \boldsymbol{O}_k^{(p)} = \boldsymbol{U}_k^{(N)} \boldsymbol{\Sigma}_k^{(N)^{1/2}} \\ \boldsymbol{Z}_k^{(m)} = \boldsymbol{\Sigma}_k^{(N)^{1/2}} \boldsymbol{V}_k^{(N)\intercal} \end{cases}. \tag{26}$$

The same procedure at time step $k+1$ will lead to

$$\tilde{\boldsymbol{H}}_{k+1}^{(p,m)} = \boldsymbol{U}_{k+1}^{(N)} \boldsymbol{\Sigma}_{k+1}^{(N)} \boldsymbol{V}_{k+1}^{(N)\intercal} = \boldsymbol{O}_{k+1}^{(p)} \boldsymbol{Z}_{k+1}^{(m)} \Rightarrow \begin{cases} \boldsymbol{O}_{k+1}^{(p)} = \boldsymbol{U}_{k+1}^{(N)} \boldsymbol{\Sigma}_{k+1}^{(N)\,1/2} \\ \boldsymbol{Z}_{k+1}^{(m)} = \boldsymbol{\Sigma}_{k+1}^{(N)\,1/2} \boldsymbol{V}_{k+1}^{(N)\intercal} \end{cases} . \tag{27}$$

Note that the state variable ensemble matrix $\boldsymbol{Z}_{k+1}^{(m)}$ at time $k+1$ is related to the state variable ensemble matrix $\boldsymbol{Z}_{k}^{(m)}$ at time k by

$$\boldsymbol{Z}_{k+1}^{(m)} = A_k \boldsymbol{Z}_{k}^{(m)} \tag{28}$$

which leads to the estimate

$$\hat{A}_k = \boldsymbol{Z}_{k+1}^{(m)} \boldsymbol{Z}_{k}^{(m)\,\dagger} \tag{29}$$

for the time-varying state matrix. The calculation of the corresponding $\hat{C}_k$ is accomplished by setting

$$\hat{C}_k = \boldsymbol{O}_{k}^{(p)}[0:N,:]. \tag{30}$$

Finally, in case the initial condition of the signal of interest is not part of the state variable ensemble at time 0, $\boldsymbol{Z}_0^{(m)}$, one needs to identify the initial condition with an additional development. Writing the general expression of the output at the initial time for an additional p more time steps, one obtain a set of equations that can be written in a matrix form as

$$\boldsymbol{\chi}_0^{(p)} = \boldsymbol{O}_0^{(p)} \boldsymbol{z}_0 \tag{31}$$

with

$$\boldsymbol{\chi}_0^{(p)} = \begin{bmatrix} \boldsymbol{\chi}_0 \\ \boldsymbol{\chi}_1 \\ \vdots \\ \boldsymbol{\chi}_{p-1} \end{bmatrix}, \quad \boldsymbol{O}_0^{(p)} = \begin{bmatrix} C_0 \\ C_1 A_0 \\ C_2 A_1 A_0 \\ \vdots \\ C_{p-1} A_{p-2} \ldots A_0 \end{bmatrix}. \tag{32}$$

Eq. (31) can be solved using the least-squares solution:

$$\hat{\boldsymbol{z}}_0 = \boldsymbol{O}_0^{(p)\,\dagger} \boldsymbol{\chi}_0^{(p)}. \tag{33}$$

This methodology based on TVERA allows one to construct a time-varying version of the Koopman operator for identifying the system matrices for an uncontrolled dynamical system. It is shown in [24] that the identified time-varying plant models that are in arbitrary coordinate systems at each time step are compatible with one another, owing the fact that they belong to the same set of experiments, hence suitable for state propagation.

IV. Numerical Simulations

This section aims to demonstrate the efficacy of the proposed approach for identifying a reduced-order model (ROM) of a nonlinear aerothermoelastic simulation. Following previous work [27], a ROM is built for a coupled thermal-structural response for the flutter of a panel with prescribed increasing temperature. This numerical simulation allows us to demonstrate the capability of the developed algorithm on a low order model where the measurements are of low dimension.

The true unknown dynamical model capturing the flutter of a heated panel is given as [41]:

$$\frac{1}{2}\pi^4 q_1(t) - 5\pi^2 R_T q_1(t) + \frac{5}{4}\pi^4 q_1^3(t) - \frac{4}{3}\lambda q_2(t) + 5\pi^4 q_1(t) q_2^2(t) + \frac{1}{2}\sqrt{\frac{\lambda\mu}{M}} q_1'(t) + \frac{1}{2} q_1''(t) = 0, \tag{34a}$$

$$\frac{4}{3}\lambda q_1(t) + 8\pi^4 q_2(t) - 20\pi^2 R_T q_2(t) + 5\pi^4 q_1^2(t) q_2(t) + 20\pi^4 q_2^3(t) + \frac{1}{2}\sqrt{\frac{\lambda\mu}{M}} q_2'(t) + \frac{1}{2} q_2''(t) = 0. \tag{34b}$$

where q_1 and q_2 are structural modal coordinates, λ is the dynamic pressure quantifying the aerodynamic loading, μ is the mass ratio quantifying the aerodynamic damping effect, R_T is the in-plane force due to the thermal stress. In general, when $R_T = 0$, there is a critical value λ_{cr}, such that the panel stays stable when $\lambda < \lambda_{cr}$, but enters limit cycle oscillation (LCO) when $\lambda > \lambda_{cr}$. When $R_T > 0$, the critical value λ_{cr} still exists. However, the panel may become statically buckled or enter chaotic response instead of being stable, when $\lambda < \lambda_{cr}$. In this example, it is assumed that $R_T = 0$ and the response of the panel is studied for a range of λ between 260 and 300. Additionally, the mass ratio and Mach number are set to $\mu = 0.01$ and $M = 5$.

For this simulation, it is desired to assess the capabilities of the time-varying Koopman operator obtained using the TVERA algorithm described in the previous section. Three different cases are considered corresponding to different orders of lifting functions to approximate the true infinite-dimensional Koopman operator with finite dimension, both for time-invariant and time-varying operators:

1) Case 1: state alone, i.e. linear basis functions in q_1, q_2, q_1' and q_2'
2) Case 2: basis function up to degree 2 in q_1, q_2, q_1' and q_2'
3) Case 3: basis functions up to degree 3 in q_1, q_2, q_1' and q_2'

The measurement data is simultaed at a frequency of 100 Hz, i.e., a time step size of 0.01s, for 10 seconds. Training trajectories are simulated by random sampling of initial deviation from a zero mean Gaussian distribution with standard deviation of 0.0001 from the nominal initial condition $\overline{\boldsymbol{q}}(0) = \begin{bmatrix} 0.001 & 0 & 0 & 0 \end{bmatrix}^{\mathsf{T}}$. For the Hankel matrix in Eq. (22) to be full rank, the number of experiments m needs to be greater than the augmented dimension N of $\boldsymbol{z}_k$. Since N is at maximum 34 for Case 3, a number of experiment $m = 100 > N$ is chosen. Simulations are performed for $260 \leq \lambda \leq 300$ with a step size of 1; hence a Koopman operator is derived for each value of λ.

Figures 2a to 2e and 3a to 3e show the identification capabilities of both the time-invariant Koopman (TI Koopman) and time-varying Koopman (TV Koopman) operators to reproduce the amplitude of the deformation modes of the panel. While the TI Koopman operator performs well before the bifurcation occurs ($\lambda < 280$), it degrades when the amplitude of the LCO increases. Particularly the model fails to capture the transient response of the panel that transitions from initial condition to LCO. On the other hand, the TVERA procedure is able to provide a linear time-varying operator that approximates the dynamics of the nonlinear system for all values of λ.

The RMS errors are presented in Figure 4 for both operators for the three cases. From Fig. 4, it is clear that the accuracy of the time-invariant as well as time-varying Koopman operators improves when the lifting degree increases. Furthermore, the TV Koopman operator provides from one to two (for large oscillations) up to five (for small oscillations) orders of magnitude better prediction accuracy than the prediction errors corresponding to the conventional TI Koopman operator. While the accuracy of the TI Koopman operator for lifted degree 3, i.e., test case 3 is comparable to actual linearization of the nonlinear equations of motion, the prediction accuracy corresponding to the TV Koopman operator is much better than its TI counterpart for lifted degree 3.

Figure 5 presents the bifurcation plot corresponding to the panel flutter problem. To generate Fig. 5, TV Koopman approximators of order 3 are calculated for each value of λ between 260 and 300. If models for some values of λ are not available, interpolated values are calculated from the two adjacent models. This method shows a very good agreement between the identified, the interpolated and the true values because amplitude of the LCO is calculated once the transient regime has vanished and the oscillatory regime settled.

There is an additional consideration for the computational efficiency of the method. To achieve sufficient accuracy, the learning of the TV Koopman operator requires trajectories that march long time beyond the onset of the LCO, so that the LCOs reach a steady state. The long time trajectory results in the computation of repeated TV Koopman operators in the invariant phase space of the LCO. To avoid such repeatitions, a library consisting of system matrices as well as the associated trajectory of the reduced order model is built from a few LCOs. Further oscillations can be predicted by propagating the state using state matrices from the library. The selection of system matrices at each step requires one to solve an optimization problem where the norm of the distance between the actual measurement vector at time k and the measurement vector from values available in the library is minimized. The resulting index will allows one to select the optimal system matrices and propagate the state for the next time step. Figure 6 summarizes the overall procedure.

V. Conclusion and Future Work

A time varying Koopman operator (TVKO) is presented to study the aerothermoeleastic analysis for a hypersonic flow. In particular, the flutter dynamics of a heated panel in a hypersonic flow is considered. A subspace identification method known as time-varying eigensystem realization algorithm (TVERA) is used to derive a finite dimensional approximation for the TVKO. The TVKO is shown to be consistent at each time step, hence suitable for state propagation.

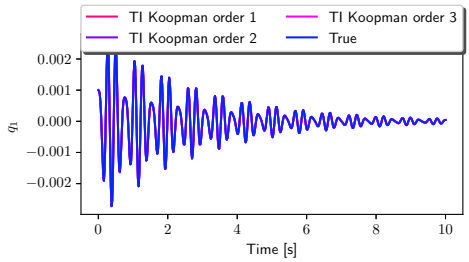

(a) q_1 **for** $\lambda = 260$

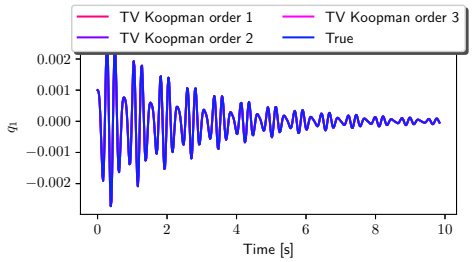

(b) q_1 **for** $\lambda = 260$

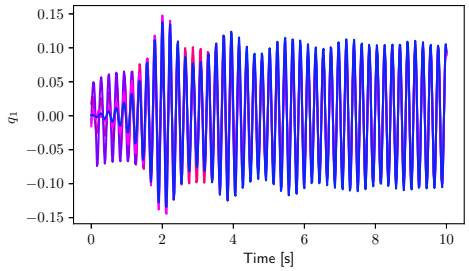

(c) q_1 **for** $\lambda = 280$

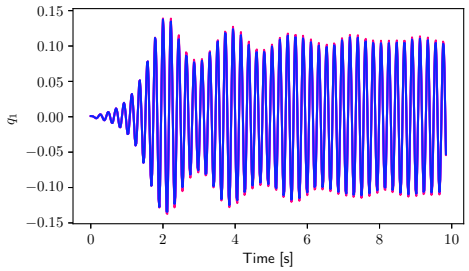

(d) q_1 **for** $\lambda = 280$

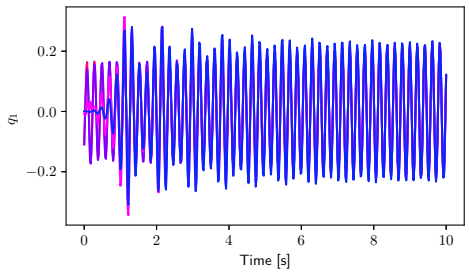

(e) q_1 **for** $\lambda = 300$

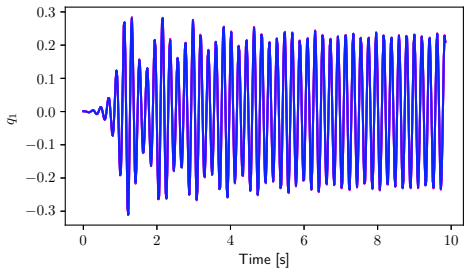

(f) q_1 **for** $\lambda = 300$

Fig. 2 Propagation of state q_1 for different values of λ. LTI Koopman on the left, LTV Koopman on the right.

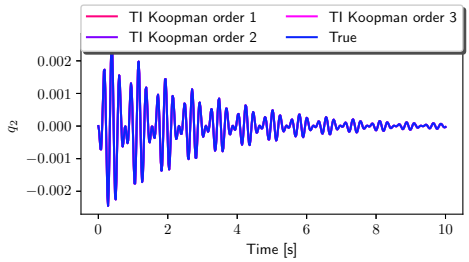

(a) q_2 **for** $\lambda = 260$

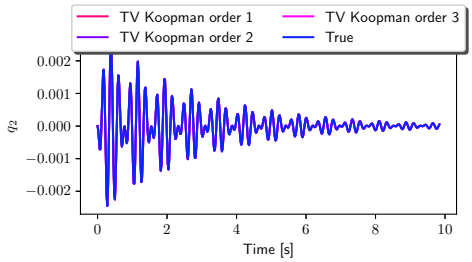

(b) q_2 **for** $\lambda = 260$

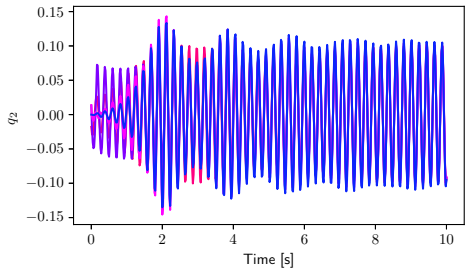

(c) q_2 **for** $\lambda = 280$

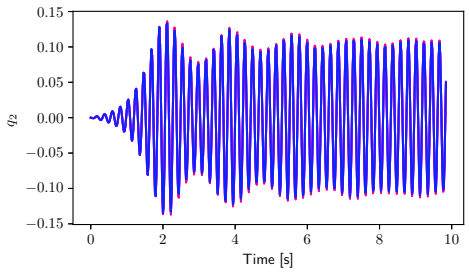

(d) q_2 **for** $\lambda = 280$

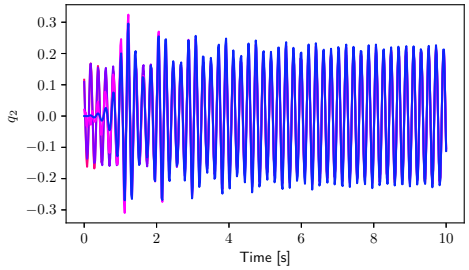

(e) q_2 **for** $\lambda = 300$

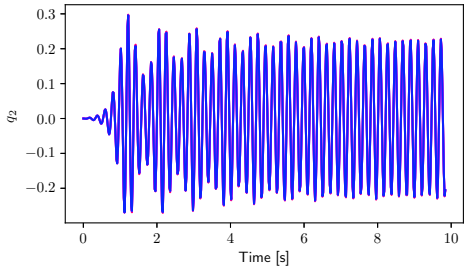

(f) q_2 **for** $\lambda = 300$

Fig. 3 Propagation of state q_2 for different values of λ. LTI Koopman on the left, LTV Koopman on the right.

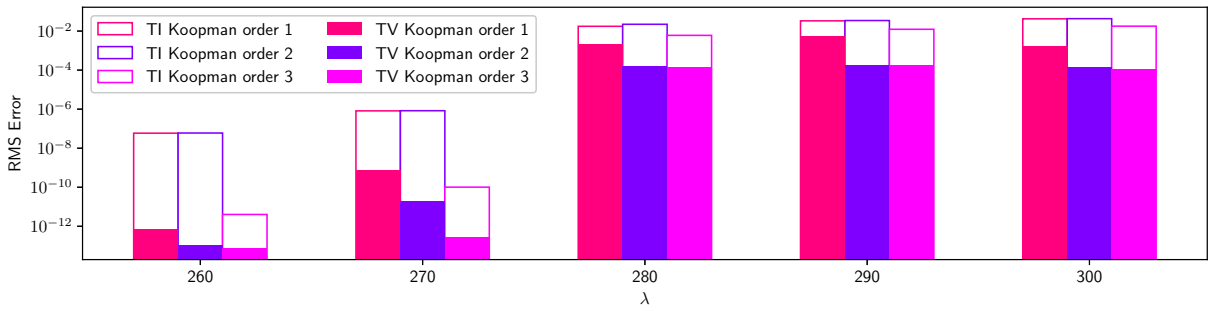

Fig. 4 RMSE of the states q_1 and q_2 for LTI and LTV Koopman for different values of λ

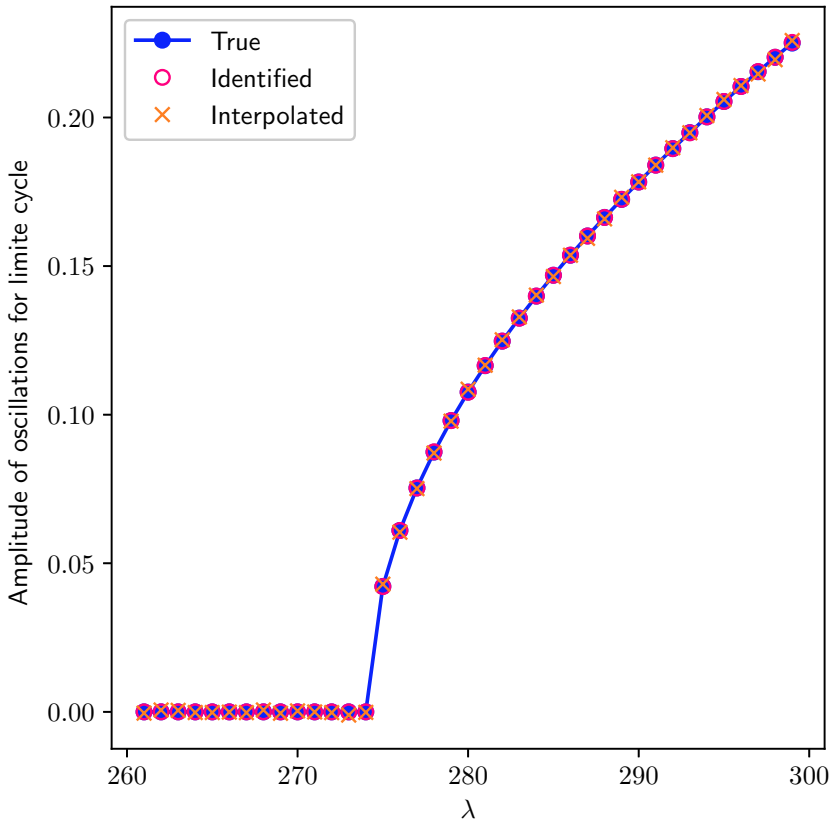

Fig. 5 Bifurcation plot

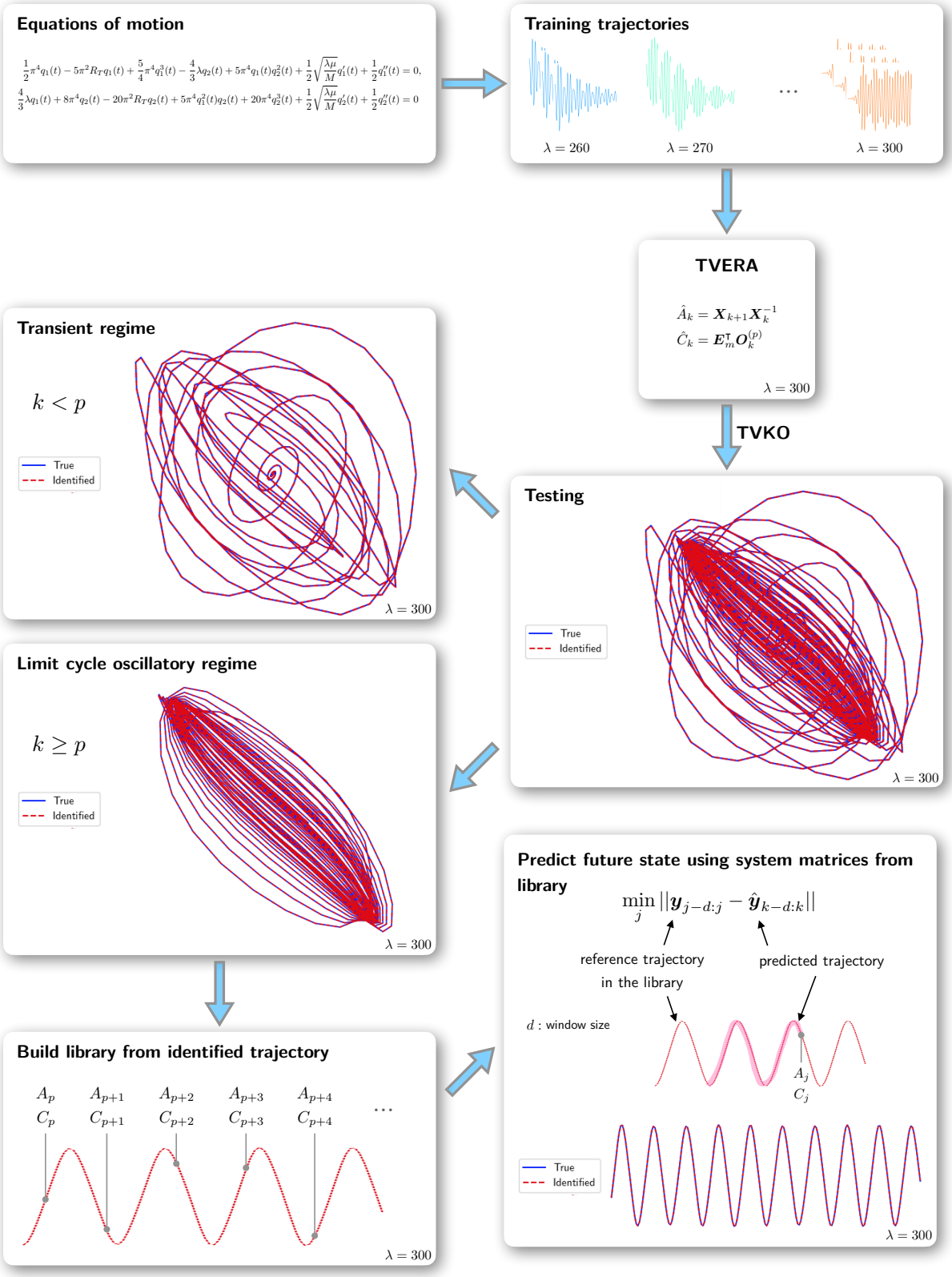

Fig. 6 Overall procedure to predict trajectory in a limit cycle

Numerical experiments corresponding to the flutter of a heated panel shows that the TVKO is able to capture the bifurcation with a good accuracy. Numerical results clearly show the improved performance of the TVKO approach as compared to conventional time-invariant Koopman operator. Additionally, a method is proposed to predict the state of a trajectory once the limit cycle oscillation regime has settled based on previous values of the system matrices in an invariant phase space. In future research work, the performance of the TVKO will be evaluated for a high-fidelity aerothermoelastic model of a skin panel.

VI. Acknowledgment

This work is supported by the AFOSR grant FA9550-20-1-0176.

References

[1] McNamara, J. J., and Friedmann, P. P., "Aeroelastic and Aerothermoelastic Analysis in Hypersonic Flow: Past, Present, and Future," *AIAA Journal*, Vol. 49, No. 6, 2011, pp. 1089–1122. doi:10.2514/1.J050882.

[2] Bowcutt, K. G., "Physics Drivers of Hypersonic Vehicle Design," *AIAA 2018–5373, 22nd AIAA International Space Planes and Hypersonics Systems and Technologies Conference*, Orlando, FL, 2018, pp. 1–22. doi:10.2514/6.2018-5373.

[3] Lamorte, N., Friedmann, P. P., Glaz, B., Culler, A. J., Crowell, A. R., and McNamara, J. J., "Uncertainty Propagation in Hypersonic Aerothermoelastic Analysis," *Journal of Aircraft*, Vol. 51, No. 1, 2014, pp. 192–203. doi:10.2514/1.C032233.

[4] Smarslok, B. P., "Quantifying Confidence in Model Predictions for Hypersonic Aircraft Structures," Tech. rep., AIR FORCE RESEARCH LAB WRIGHT-PATTERSON AFB OH AEROSPACE SYSTEMS DIRECTORATE, 2015.

[5] Huang, D., "Development of a Hypersonic Aerothermoelastic Framework and Its Application to Flutter and Aerothermoelastic Scaling of Skin Panels," Ph.D. thesis, University of Michigan, Ann Arbor, 2019.

[6] Culler, A. J., and McNamara, J. J., "Impact of Fluid-Thermal-Structural Coupling on Response Prediction of Hypersonic Skin Panels," *AIAA Journal*, Vol. 49, No. 11, 2011, pp. 2393–2406. doi:10.2514/1.J050617.

[7] Falkiewicz, N. J., and Cesnik, C. E., "Enhanced Modal Solutions for Structural Dynamics in Aerothermoelastic Analysis," *Journal of Aircraft*, Vol. 54, No. 3, 2017, pp. 870–889.

[8] Huang, D., and Friedmann, P. P., "An Aerothermoelastic Analysis Framework with Reduced-Order Modeling Applied to Composite Panels in Hypersonic Flows," *Journal of Fluids and Structures*, 2020.

[9] Koopman, B. O., "Hamiltonian Systems and Transformation in Hilbert Space," *Proceedings of the National Academy of Sciences*, Vol. 17, No. 5, 1931, pp. 315–318.

[10] Koopman, B. O., and Neumann, J.-V., "Dynamical Systems of Continuous Spectra," *Proceedings of the National Academy of Sciences*, Vol. 18, No. 3, 1932, pp. 255–263.

[11] Mezić, I., and Banaszuk, A., "Comparison of systems with complex behavior," *Physica D: Nonlinear Phenomena*, Vol. 197, 2004, pp. 101–133.

[12] Mezić, I., "Spectral Properties of Dynamical Systems, Model Reduction and Decompositions," *Nonlinear Dynamics*, Vol. 41, 2005, pp. 309–325.

[13] Korda, M., and Mezic, I., "Linear predictors for nonlinear dynamical systems: Koopman operator meets model predictive control," *Automatica*, Vol. 93, 2018, pp. 149–160.

[14] Brunton, S. L., Brunton, B. W., Proctor, J. L., and Kutz, J. N., "Koopman Invariant subspaces and Finite Linear Representations of Nonlinear Dynamical Systems for Control," *PLoS ONE*, Vol. 11, No. 1, 2016, p. e0150171.

[15] Williams, M. O., Kevrekidis, I. G., and Rowley, C. W., "A Data–Driven Approximation of the Koopman Operator: Extending Dynamic Mode Decomposition," *Journal of Nonlinear Science*, Vol. 25, 2015, pp. 1307–1346.

[16] Schmid, P. J., "Dynamic mode decomposition of numerical and experimental data," *Journal of Fluid Mechanics*, Vol. 656, 2010, pp. 5–28.

[17] Tu, J. H., Rowley, C. W., Luchtenburg, D. M., Brunton, S. L., and Kutz, J. N., "On Dynamic Mode Decomposition: Theory and Applications," *Journal of Computational Dynamics*, Vol. 1, No. 2, 2014, pp. 391–421.

[18] Williams, M. O., Kevrekidis, I. G., and Rowley, C. W., "A data–driven approximation of the koopman operator: Extending dynamic mode decomposition," *Journal of Nonlinear Science*, Vol. 25, No. 6, 2015, pp. 1307–1346.

[19] Shokoohi, S., and Silverman, L. M., "Identification and Model Reduction of Time-varying Discrete-time Systems," *Automatica*, Vol. 23, No. 4, 1987, pp. 509–521.

[20] Dewilde, P., and Van Der Veen, A. J., *Time Varying Systems and Computations*, Kluwer Academic Publisher, 1998.

[21] Verhaegen, M., *Identification of Time-Varying State Space Models from Input-Output Data*, Workshop on Advanced Algorithms and their Realization, Bonas, 1991.

[22] Liu, K., "Identification of Linear Time-Varying Systems," *Journal of Sound and Vibration*, Vol. 206, No. 4, 1997, pp. 487–505.

[23] Liu, K., "Extension of Modal Analysis to Linear Time Varying Systems," *Journal of Sound and Vibration*, Vol. 226, No. 1, 1999, pp. 149–167.

[24] Majji, M., Juang, J.-N., and Junkins, J. L., "Time-Varying Eigensystem Realization Algorithm," *Journal of Guidance, Control, and Dynamics*, Vol. 33, No. 1, 2010, pp. 13–28. doi:https://doi.org/10.2514/1.45722.

[25] Majji, M., Juang, J.-N., and Junkins, J. L., "Observer/Kalman-Filter Time-Varying System Identification," *Journal of Guidance, Control, and Dynamics*, Vol. 33, No. 3, 2010, pp. 887–900. doi:https://doi.org/10.2514/1.45768.

[26] Zhang, H., Rowley, C. W., Deem, E. A., and Cattafesta, L. N., "Online Dynamic Mode Decomposition for Time-Varying Systems," *SIAM Journal on Applied Dynamical Systems*, Vol. 18, No. 3, 2019, pp. 1586–1609.

[27] Guého, D., Singla, P., and Majji, M., "Time-Varying Koopman Operator Theory for Nonlinear Systems Prediction," IEEE Conference on Decision and Control, 2021.

[28] Govindarajan, N., Mohr, R., Chandrasekaran, S., and Mezić, I., "On the approximation of Koopman spectra of measure-preserving flows," , 2018.

[29] Rowley, C. W., MEZI?, I., Bagheri, S., Schlatter, P., Henningson, D., et al., "Spectral analysis of nonlinear flows," *Journal of fluid mechanics*, Vol. 641, No. 1, 2009, pp. 115–127.

[30] Georgescu, M. V., and Mezic, I., "Improving hvac performance through spatiotemporal analysis of building thermal behavior," 2014.

[31] Susuki, Y., and Mezić, I., "Nonlinear Koopman Modes and Power System Stability Assessment Without Models," *IEEE Transactions on Power Systems*, Vol. 29, No. 2, 2014, pp. 899–907. doi:10.1109/TPWRS.2013.2287235.

[32] Proctor, J., and Welkhoff, P., "Discovering dynamic patterns from infectious disease data using dynamic mode decomposition," *International health*, Vol. 7, 2015, pp. 139–45. doi:10.1093/inthealth/ihv009.

[33] Peitz, S., Otto, S. E., and Rowley, C. W., "Data-driven model predictive control using interpolated Koopman generators," *SIAM Journal on Applied Dynamical Systems*, Vol. 19, No. 3, 2020, pp. 2162–2193.

[34] Juang, J.-N., and Pappa, R. S., "An Eigensystem Realization Algorithm (ERA) for Modal Parameter Identification and Model Reduction," *Journal of Guidance, Control, and Dynamics*, Vol. 8, No. 5, 1985, pp. 620–627. doi:https://doi.org/10.2514/3.20031.

[35] Juang, J.-N., Cooper, J. E., and Wright, J. R., "An Eigensystem Realization Algorithm Using Data Correlation (ERA/DC) for Modal Parameter Identification," *Control Theory and Advanced Technology*, Vol. 4, No. 1, 1988, pp. 5–14.

[36] Kutz, J. N., Brunton, S. L., Brunton, B. W., and Proctor, J. L., *Dynamic Mode Decomposition: Data-Driven Modeling of Complex Systems*, SIAM, 2016.

[37] Rowley, C. W., Mezic, I., Bagheri, S., Schlatter, P., and Henningson, D., "Spectral analysis of nonlinear flows," *Journal of Fluid Mechanics*, Vol. 641, 2009, pp. 115–127.

[38] Cho, Y. M., Xu, G., and Kailath, T., "Fast Recursive Identification of State Space Models via Exploitation of Displacement Structure," *Automatica*, Vol. 30, No. 1, 1994, pp. 45–59.

[39] Sayadi, T., Schmid, P. J., Richecoeur, F., and Durox, D., "Parametrized data-driven decomposition for bifurcation analysis, with application to thermo-acoustically unstable systems," *Physics of Fluids*, Vol. 27, No. 3, 2015, p. 037102.

[40] Verhaegen, M., and Yu, X., "A Class of Subspace Model Identification Algorithms to Identify Periodically and Arbitrarily Time Varying Systems," *Automatica*, Vol. 31, No. 2, 1995, pp. 201–216. doi:https://doi.org/10.1016/0005-1098(94)00091-V.

[41] Dowell, E. H., *Aeroelasticity of Plates and Shells*, Noordhoff International Publishing, Leyden, 1974.